D. E. Waliser · Z. Shi · J. R. Lanzante · A. H. Oort

The Hadley circulation: assessing NCEP/NCAR reanalysis and sparse in-situ estimates

Abstract We present a comparison of the zonal mean meridional circulations derived from monthly in situ data (i.e. radiosondes and ship reports) and from the NCEP/NCAR reanalysis product. To facilitate the interpretation of the results, a third estimate of the mean meridional circulation is produced by subsampling the reanalysis at the locations where radiosonde and surface ship data are available for the in situ calculation. This third estimate, known as the subsampled estimate, is compared to the complete reanalysis estimate to assess biases in conventional, in situ estimates of the Hadley circulation associated with the sparseness of the data sources (i.e., radiosonde network). The subsampled estimate is also compared to the in situ estimate to assess the biases introduced into the reanalysis product by the numerical model, initialization process and/or indirect data sources such as satellite retrievals. The comparisons suggest that a number of qualitative differences between the in situ and reanalysis estimates are mainly associated with the sparse sampling and simplified interpolation schemes associated with in situ estimates. These differences include: (1) a southern Hadley cell that consistently extends up to 200 hPa in the reanalysis, whereas the bulk of the circulation for the in situ and subsampled estimates tends to be confined to the lower half of the troposphere, (2) more well-defined and consistent poleward limits of the Hadley cells in the reanalysis compared to the in-situ and subsampled estimates, and (3) considerably less variability in magnitude and latitudinal extent of the Ferrel cells and southern polar cell exhibited in the reanalysis estimate compared to the in situ and subsampled estimates. Quantitative comparison shows that the subsampled estimate, relative to the reanalysis estimate, produces a stronger northern Hadley cell ($\sim$20%), a weaker southern Hadley cell ($\sim$20–60%), and weaker Ferrel cells in both hemispheres. These differences stem from poorly measured oceanic regions which necessitate significant interpolation over broad regions. Moreover, they help to pinpoint specific shortcomings in the present and previous in situ estimates of the Hadley circulation. Comparisons between the subsampled and in situ estimates suggest that the subsampled estimate produces a slightly stronger Hadley circulation in both hemispheres, with the relative differences in some seasons as large as 20–30%. These differences suggest that the mean meridional circulation associated with the NCEP/NCAR reanalysis is more energetic than observations suggest. Examination of ENSO-related changes to the Hadley circulation suggest that the in situ and subsampled estimates significantly overestimate the effects of ENSO on the Hadley circulation due to the reliance on sparsely distributed data. While all three estimates capture the large-scale region of low-level equatorial convergence near the dateline that occurs during El Nino, the in situ and subsampled estimates fail to effectively reproduce the large-scale areas of equatorial mass divergence to the west and east of this convergence area, leading to an overestimate of the effects of ENSO on the zonal mean circulation.

D. E. Waliser (✉) · Zhixiong Shi[1]
Institute for Terrestrial and Planetary Atmospheres,
State University of New York,
Stony Brook, NY 11794-5000, USA
E-mail: waliser@terra.MSRC.Sunysb.EDU

Present address:
[1]SAIC/GSC MODIS Support Office,
7501 Forbes Blvd., Suite 101, Greenbelt, MD 20706, USA

J. R. Lanzante · A. H. Oort
Geophysical Fluid Dynamics Laboratory,
Princeton University, Princeton, NJ 08542, USA

1 Introduction

As observations of the atmospheric circulation began to accumulate, scientists began to develop theories to explain the observed features. As the observations

became more plentiful, it was possible to hold these theories to more rigorous constraints. This would often lead to improved theories that could better account for the observed wind patterns. This interplay between observations and general circulation theory essentially began with Hadley's (1735) attempt to explain the easterly winds in the tropics. Using the principle of angular momentum conservation along with a general understanding of the distribution of solar heating, Hadley's theory accounted for the easterly "trade winds". In addition, his theory suggested that the mean meridional circulation consisted of overall rising motion in lower latitudes and a sinking motion in higher latitudes with the completion of this circuit produced by equatorward motion at low levels and poleward motion aloft. While some aspects of Hadley's theory needed modification, the fact that it aptly described the zonal-mean meridional circulation in the tropics is the basis for this circulation bearing his name today. (Lorenz (1967) provides a thorough and illuminating history of the early developments of the theory of the general circulation.) The concept of the Hadley circulation has been extremely useful for those studying tropical and even mid-latitude climate, and in recent times it most often serves as an important diagnostic for climate and numerical weather prediction models.

Over the last 50 y the atmospheric circulation has been sampled with considerably more detail, especially with respect to upper level winds. This has allowed more complete observational descriptions of the climatology and variability of the zonal-mean meridional circulation. Such studies include Oort and Rasmusson (1970), Newell et al. (1972), Oort (1983) and Oort and Yienger (1996). Results from these observational studies indicate that the mean meridional circulation typically shows a three-cell pattern from the equator poleward, with a strong Hadley cell in the tropics, a weak Ferrel cell in the midlatitudes, and an even weaker polar cell in the high latitudes. The increased level of detail and confidence these observational studies have provided have continued to foster theoretical arguments (Schneider and Lindzen 1977; Schneider 1977; Held and Hou 1980; Schneider 1987; Hack et al. 1989; Emanuel 1995). For example, the observational descriptions show that during solstice periods, the winter hemisphere cells of the three-cell structure typically dominate, particularly in the case of the wintertime Hadley cell which extends well into the summer hemisphere. Only in the last decade or two has this feature begun to be directly addressed by theory (Lindzen and Hou 1988; Hou and Lindzen 1992)

While the observational studies had considerably more data to rely on than did those of a century earlier (e.g., Maury 1855; Buchan 1889), they are still based on data that are severely limited in space and often in time as well. While many factors introduce errors into the observations which can limit and/or obscure our description of the atmospheric circulation (Trenberth and

Olson 1989; Elliot and Gaffen 1991; Schwartz and Doswell 1991; Gaffen 1994; Parker and Cox 1995), for studies of interannual variability it is likely that the spatial gaps in the observation network represent the most significant error, even for the data-dense Northern Hemisphere (e.g. Oort 1978; Soden and Lanzante 1996). At present, the most data-sparse areas are the tropical oceans and the vast open-ocean areas of the Southern Hemisphere. Moreover, the number of upper air radiosondes has been declining since reaching a peak during the Global Weather Experiment in 1979. Overcoming these observational shortcomings will continue to be a challenge in assessing the nature and variability of the general circulation. The recently emerging reanalysis projects (e.g. Kalney et. al. 1996; Schubert et. al. 1993; European Centre for Medium-Range Weather Forecasts, Reading, UK) may be a good approach to help solve this problem due to the numerous sources of observations that are utilized (e.g. radiosondes, surface ship reports, drifting and moored buoys, satellite observations, etc.). However, since the production of these reanalysis data sets relies on data assimilation systems with known shortcomings and numerical models that heavily parametrize some physical processes, they are also subject to considerable uncertainties and biases.

The objective of this study is to compare estimates of the Hadley circulation produced from a long-record reanalysis product, in this case the National Centers for Environmental Prediction/National Center for Atmospheric Research (NCEP/NCAR) reanalysis project (Kalnay et al. 1996), to that produced from in situ observations using traditional techniques (i.e., radiosonde wind data with some form of objective analysis). However, since both of these estimates suffer from their own biases and uncertainties, the process of producing a meaningful comparison with useful and meaningful inferences is not straightforward. For example, differences between these two estimates could be attributable to either the sparseness of the data which is the most severe shortcoming in the in situ estimate, or they could be attributable to the biases introduced by the initialization procedures and model physical parametrizations which could be thought of as the most severe shortcomings of the reanalysis data set. To overcome this limitation, we have chosen to produce a third estimate by subsampling the reanalysis data set at the locations where observed data exist, and then estimate the Hadley circulation from this subset of data in the same way the in situ estimate is produced. This third estimate suffers from both the sparse data limitation as well as the biases from the numerical analysis procedures. By comparing the subsampled and reanalysis estimates, one can draw inferences regarding the biases in the conventional in situ estimates due to sparseness of the data sources (i.e., radiosonde network). By comparing the subsampled and in situ estimates, inferences may be drawn regarding the biases in the reanalysis

estimates due to the numerical analyses. With regards to the latter, it is important to remember that these model biases are assessed where actual in situ observations exist and it is likely that they would be an underestimate, or possibly not altogether apply, to regions void of in situ data.

In the next section, the data sets used in this study are discussed. In Sect. 3, the methods used to obtain the in situ, reanalysis and subsampled estimates of the Hadley circulation are discussed. In Sect. 4, the results of the computations and comparisons are presented. Finally, a summary and discussion are presented in Sect. 5.

2 Data

The in situ estimate of the Hadley circulation is computed from a combination of monthly averaged radiosonde data and monthly averaged surface wind data from the Comprehensive Ocean-Atmosphere Dataset (COADS; Woodruff et al. 1987). The radiosonde data set was compiled at the Geophysical Fluid Dynamics Laboratory (GFDL). This is an updated version of the GFDL Atmospheric Circulation Tape Library described in Oort (1983) which extends to 1989. While this data set includes 06Z and 18Z reports, their total number is significantly fewer than the number of 00Z and 12Z reports, and thus in this study only the 00Z and 12Z data were used. The first column in Table 1 lists the pressure levels available in this data set. Due to a marked amount of missing data at a number of levels prior to 1968, our analysis includes data only from the period 1968 to 1989. Furthermore, only levels/stations that reported for at least 10 days for a given month were used in the analysis. The second

column in Table 1 shows the total number of monthly observations that meet this criterion for each level. Following Oort and Yienger (1996), the monthly meridional wind data from COADS are used to supplement the near-surface analysis over oceanic regions.

The reanalysis estimate of the Hadley circulation is computed from monthly NCEP/NCAR reanalysis data. These data have a horizontal resolution of 2.5° latitude by 2.5° longitude, are provided on 17 unevenly spaced pressure levels (see fourth column of Table 1), and are generated with a time resolution of 6 h. Our analysis utilizes only the 00Z and 12Z periods to be consistent with the radiosonde sampling and to limit the influence from atmospheric tides. Trenberth (1991), Trenberth and Solomon (1994) and van den Dool et al. (1997) have shown that the semi-diurnal tide produces a weak but coherent wave number two surface pressure signal which is primarily confined to the tropics. The diurnal period of this propagating signal results in an in-phase relationship for the surface pressure and vertical velocity fields at 00Z and 12Z, likewise for the 06Z and 18Z, but an out-of-phase relationship for periods separated by 6 h. In addition to the 17 standard levels shown in Table 1, the 10 m wind field is used as a representation of the near-surface wind field and is meant to be analogous to the wind field information provided by COADS for use over the ocean by the in situ analyses.

Finally, the "Nino 3.4" sea surface temperature (SST) anomaly time series is used as a measure of El Nino Southern Oscillation (ENSO) variability. The Nino 3.4 region extends from 5°S–5°N and 170°–120°W and the anomaly is computed with respect to the annual cycle.

3 Methods

Three estimates of the Hadley circulation are computed and analyzed. One is computed directly from the in situ data sources (i.e.,

Table 1 Pressure (hPa) levels in the original monthly radiosonde data (1st column) and the levels used in the in situ (3rd column), reanalysis (4th column), and subsampled (4th column) estimates of the Hadley circulation. The total number of monthly 00Z and 12Z reports (having at least 10 observations during a month) at each in situ level (2nd column)

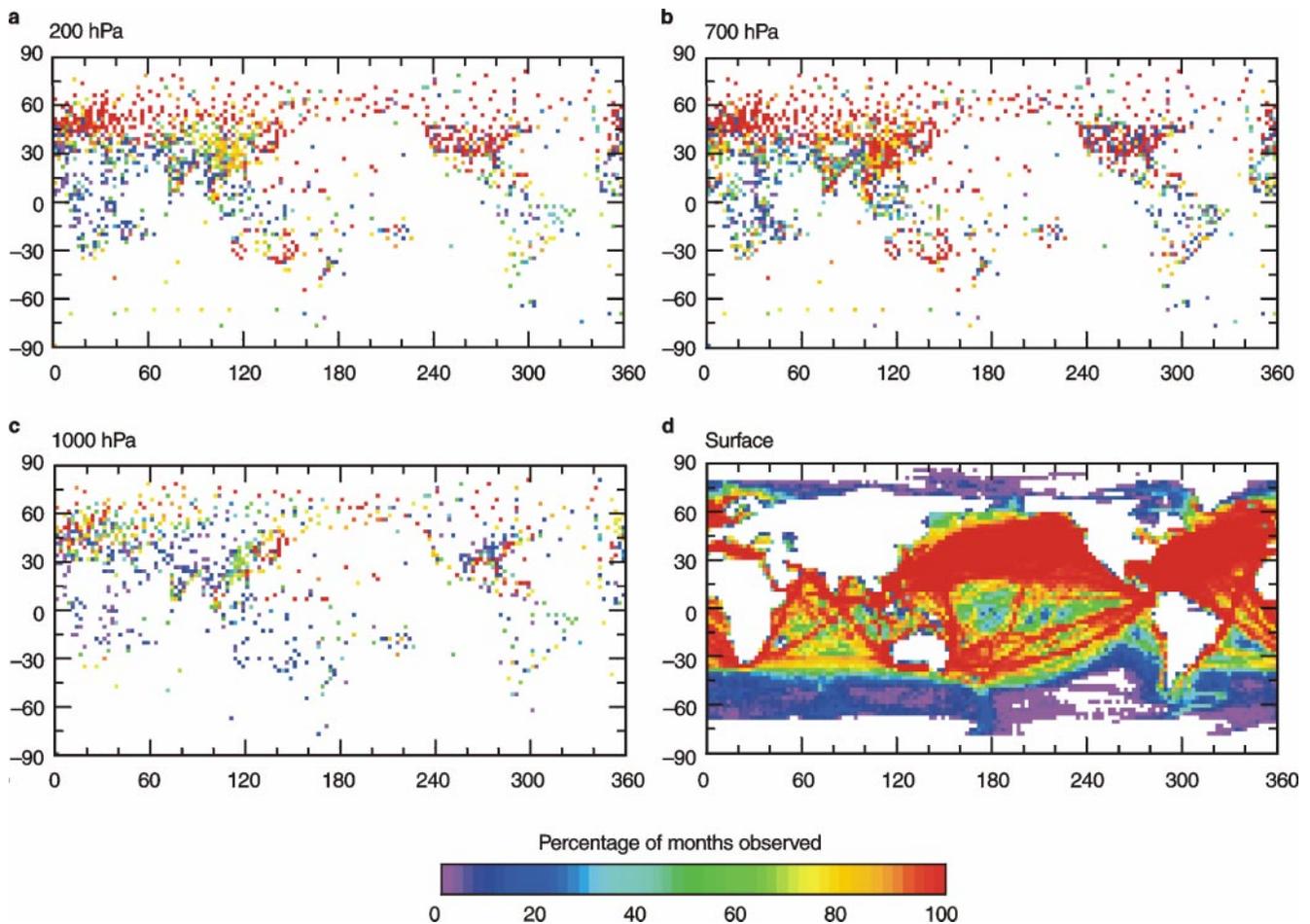| Radiosonde Data	Number of 00Z + 12Z Reports	In-Situ Analysis	Renalysis and Subsampled Analyses
7	806		
10	50,272		10
15	50,942		
20	173,064	20	20
30	221,468	30	30
50	250,805	50	50
70	265,266	70	70
100	327,445	100	100
150	343,476	150	150
200	359,391	200	200
250	364,851	250	250
300	376,702	300	300
350	374,009	350	
400	389,551	400	400
450	384,001	450	
500	419,980	500	500
550	322,298	550	
600	321,902	600	600
650	321,363	650	
700	467,537	700	700
750	351,097	750	
800	349,520	800	
850	490,061	850 (0.25)	850 (0.25)
900	270,720	900 (0.50)	
			925 (0.625)
950	249,335	950 (0.75)	
1000	190,663	1000 (1.00)	1000 (1.00)
		Surface-COADS	10-meters

Fig. 1 a–d Spatial distribution of the NCEP/NCAR reanalysis grid points where radiosonde stations existed in the GFDL/Oort monthly data set (see Sect. 2) for the **a** 200 hPa, **b** 700 hPa and **c** 1000 hPa levels and the temporal frequency these grid points were sampled over the 264 month period analyzed (1968–89). **d** Shows the same information but for the monthly averaged COADS surface reports of meridional wind

monthly radiosonde and COADS surface wind data), one is computed directly from the reanalysis data, and the third is computed from the reanalysis data subsampled at the same locations for which in situ data are available. The subsampling is performed as follows. For each month, all the reanalysis grid points that have at least one corresponding monthly radiosonde observation (made up of 10 or more daily observations) within their spatial domain are retained with the data at all other grid points flagged as missing. Note that "spatial domain" implies height (i.e. level) as well, and thus the subsampling varies with pressure level as well as with time and horizontal location. In the case of the 925 hPa level (see Table 1), if an observation exists at either the 900 hPa or 950 hPa level, then the corresponding 925 hPa reanalysis point is retained. This sampling procedure is performed using the 00Z and 12Z data separately for each month and then the results are averaged together. In a similar manner, the 10 m surface wind field from the reanalysis is also sampled using locations where monthly COADS meridional wind reports are available. Figure 1a–c shows the spatial distribution of the reanalysis grid points where radiosonde stations existed for the 200 hPa, 700 hPa and 1000 hPa levels and the temporal frequency these grid points were sampled over the 264 month period analyzed. Figure 1d shows similar information but for the monthly averaged COADS reports of meridional wind.

An updated version of the objective analysis scheme described in Oort (1983), referred to as ANAL95, is used to convert both the irregularly-spaced in situ data and the subsampled reanalysis data to the regular 2.5° reanalysis grid. This optimal interpolation scheme is based on an iterative solution of Poisson's equation and is the same scheme used by Oort and Yienger (1996). For both the in situ and subsampled cases, a 12-month climatology is first created from the two data sets, keeping only mean-monthly values having at least 10 monthly observations. An interpolation is first performed on this (sparse) 12-month annual cycle data using the zonal mean of each month as the first-guess value for missing data points. Then an interpolation for the monthly data is performed using these interpolated monthly-mean data as the first-guess values for missing data points. This interpolation procedure is performed for each level of data separately, including the surface wind level, i.e., on the COADS data for the in situ estimate and on the 10 m level winds for the subsampled reanalysis estimate.

The final step in producing the analyzed wind fields from the in situ and subsampled data sets is to merge the interpolated (ocean-based) surface winds into the rest of the analyses. The purpose of this merging is to maximize the usefulness of the ocean surface wind data in the final analyzed wind product. Oort and Yienger (1996) used the COADS-interpolated data directly for the 1000 hPa level over the ocean, and the radiosonde-interpolated data for the 1000 hPa level over land. In their case, horizontal interpolations were only done on significant levels (e.g., 1000 hPa, 850 hPa, etc.) and the intervening levels, such as the 950 hPa and 900 hPa levels, were produced by

vertical interpolation. In this study, the same procedure was used to produce the 1000 hPa level, with the ocean surface winds coming from COADS for the in situ case and the 10 m winds for the subsampled case. However, in the present study, horizontal interpolations were performed for all the levels shown in the third column of Table 1 for the in situ data and the fourth column of Table 1 for the subsampled estimate. To increase the utility of the available in situ data, the effects of the surface wind over the ocean were propagated into the near-surface levels using a weighted average of the horizontally interpolated 1000 hPa level wind (i.e., COADS or 10 m winds) and the horizontally interpolated "station" data at the given pressure level. The weights given to the surface data are shown between the parenthesis in the lowest four (three) rows of the third (fourth) column of Table 1. For example, for both data sets, the 850 hPa level data over the ocean is computed using a weighting of 0.25 for the surface data and 0.75 for the 850 hPa interpolation of the radiosonde data.

Performing these procedures provides three estimates of the monthly averaged meridional wind field, one from the reanalysis, one from the in situ data, and one from the subsampled version of the reanalysis. From these estimates of the meridional wind, the Hadley mass transport is computed by using the zonally averaged mass continuity equation in the form:

$$\frac{\partial [\bar{v}] \cos \phi}{R \cos \phi \, \partial \phi} + \frac{\partial [\bar{\omega}]}{\partial p} = 0, \tag{1}$$

where v is the meridional velocity, ω is the vertical velocity in pressure coordinates, R is the mean radius of the earth, and p is the pressure. The operators "$\bar{}$" and "[ ]" represent temporal (i.e. monthly) and zonal averaging, respectively. The form of the zonally averaged continuity Eq. (1) allows the definition of a two-dimensional streamfunction ψ, defined by the following equations:

$$[\bar{v}] = g \frac{\partial \psi}{2\pi R \cos \phi \, \partial p} \tag{2}$$

$$[\bar{\omega}] = -g \frac{\partial \psi}{2\pi R^2 \cos \phi \, \partial \phi} \tag{3}$$

which can then be used to compute the ψ field by specifying appropriate boundary conditions. In this study, we specify $\psi = 0$ at the top of the atmosphere ($P_{TOA} = 10$ hPa for the reanalyses and 20 hPa for the in situ estimates; see Table 1) and integrate downward to the surface (1000 hPa), giving:

$$\psi = \int \frac{2\pi R \cos \phi}{g} [\bar{v}] \, dp \tag{4}$$

Further, we assume there is no net mass flow across a meridian on monthly time scales. To impose this constraint, we removed the mass-weighted vertical mean values of $[\bar{v}]$, defined as:

$$\overline{[\bar{v}]} = \frac{1}{1000 - P_{TOA}} \int_{1000}^{P_{TOA}} [\bar{v}] \, dp, \tag{5}$$

from every latitudinal grid point. The statistics and structure of these residual values as a function of latitude will be described in Sect. 4b.

4 Results

4.1 Climatology

Figure 2 shows the in situ derived Hadley circulation climatology in terms of the January, April, July and October mean-monthly values as well as the long-term mean. As expected from the results of previous in situ
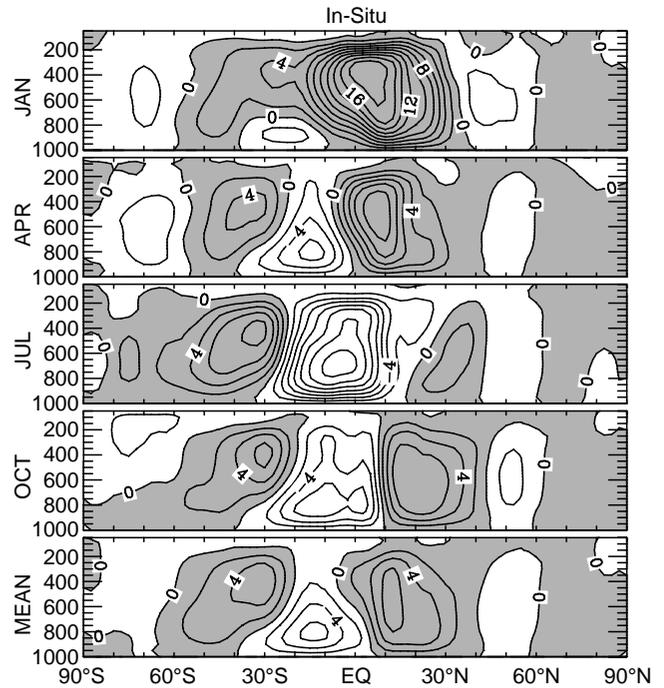

Fig. 2 Zonal-mean mass stream function derived from in situ data sources (see Sects. 2 and 3) for mean January, April, July and October conditions as well as the long-term mean for the period 1968–89. Units are in 10^{10} kg s^{-1} and the contour level is 2×10^{10} kg s^{-1}

estimates, the meridional circulation during the solstice periods is dominated by the winter hemisphere Hadley cells, with weak or non-existent summer hemisphere cells (see Lindzen and Hou 1988). The maximum values of these solstice winter hemisphere Hadley cells is about 20×10^{10} kg s^{-1} for January and about -14×10^{10} kg s^{-1} for July. During the equinox periods, the meridional circulation is significantly more symmetric, with the summer and winter Hadley cells both having maximum values on the order of ± 6 to 9×10^{10} kg s^{-1}. The long-term mean Hadley circulation has maximum values of -6.5×10^{10} kg s^{-1} and 7×10^{10} kg s^{-1} for the Southern and Northern Hemisphere Hadley cells, respectively. The structure and variability of the Ferrel cells for this in situ estimate are considerably different between the Northern and Southern hemispheres. The Ferrel cell in the Northern Hemisphere is nearly always present but very weak, with maximum values of about -2×10^{10} kg s^{-1}. The Ferrel cell in the Southern Hemisphere also tends to be present throughout the year, however it is considerably stronger, with maximum values ranging between 3×10^{10} kg s^{-1} in January and 9×10^{10} kg s^{-1} in July. It is also worth noting that the southern Ferrel cell has a large meridional extent, ranging between 25°–60°S, while the northern Ferrel cell is generally limited to 45°–60°N. Finally, the in situ estimate shows that only the Southern Hemisphere exhibits a polar cell, and this

is a very weak cell limited to the Southern Hemisphere summer and fall seasons. Based on the data in Fig. 1, it is apparent that very little observational data are available in the midlatitude and polar portions of the Southern Hemisphere, thus the level of confidence in the meridional circulation estimates in these regions is quite low. Further discussion of the uncertainties will be given later.

The in situ estimate of the Hadley circulation, computed from 22 y of data, is similar to those produced from previous estimates. As expected, the results are very similar to those presented by Oort and Yienger (1996) since the source of data is the same, the period analyzed is similar (their analysis began in 1964), and the methods are nearly identical. A comparison of their long-term mean Hadley circulation using just the period between 1968 to 1989 to the in situ estimate analyzed here shows that the northern Hadley cell in the present calculation is slightly broader in its meridional extent but its maximum value is about 15% weaker, and the southern Hadley cell is nearly identical in magnitude and meridional extent but is slightly more confined to the lower atmosphere. These differences are on the order of those expected based on the interannual variability in this type of estimate, which will be discussed in the next subsection.

There are some considerable differences between the in situ Hadley estimates shown here and those from earlier studies. For example, the study by Oort and Rasmusson (1970) used data from a 5-y period (May 1958 to April 1962) to compute the zonal-mean meridional wind field and the associated Hadley circulation. Their Hadley estimates differ from those presented in Fig. 2 primarily due to the greater strength of their southern Hadley cell which had maximum values of about -12, -23, -15 and -10×10^{10} kg s^{-1} for the April, July, October and long-term means, respectively. These values are about double the values shown here. Note however that their study domain extended only to 15 °S due to the extremely limited amount of data available south of this latitude, which is likely to contribute considerable uncertainty to their southern Hadley cell. The maximum values of their Northern Hemisphere Hadley cells were about 22, 16, 7 and 7 $\times 10^{10}$ kg s^{-1} for the January, April, October and long-term means, respectively. These values are in considerably better agreement with the estimates shown in Fig. 2. The study by Newell et al. (1972) extended from pole to pole and used a disparate set of data sources for the mid-latitudes and a 7.5 y radiosonde data set for the tropics (July 1957 and December 1964). Like Oort and Rasmusson's (1970) result, their southern Hadley cell is also considerably stronger than that shown in Fig. 2, having maximum values of about -7, -20, and -9×10^{10} kg s^{-1} for the MAM, JJA and SON means, respectively. These values are on the order of 25–35% larger than the associated mean monthly values shown here. The maximum values of their Northern Hemi-

sphere Hadley cells were about 18, 8, 5 $\times 10^{10}$ kg s^{-1} for the DJF, MAM, and SON means, respectively. These values are a bit smaller but still comparable to those shown in Fig. 2. Newell et al.'s (1972) northern Ferrel cell was relatively stable in latitudinal extent and magnitude, having maximum values ranging between about 2 and 4 $\times 10^{10}$ kg s^{-1}, reasonably similar to the magnitudes shown here. Their southern Ferrel cell showed even less variability having a value of about 3 $\times 10^{10}$ kg s^{-1} throughout the year, which is considerably weaker than the values shown here, especially in the northern summer and fall seasons.

Figure 3 shows the reanalysis derived Hadley circulation climatology. Overall, the structure of the meridional circulation is quite similar to the in situ derived estimate although there are a number of notable differences. First, the southern Hadley cell tends to be stronger in nearly all seasons, especially during January and July. In addition, the southern Hadley cells in the reanalysis shows that this cell consistently extends up to 200 hPa, whereas the bulk of the circulation for the in situ estimate tends to be confined to the lower half of the troposphere for all cases shown except July. The greater depth of the southern Hadley cell occurs in association with a more confined northern cell in the upper troposphere, especially in the January, April and long-term means. The reanalysis also shows more well-defined and consistent poleward limits of the Hadley cells, with the main regions of subsidence almost always occurring at 30 °N and 30 °S. In contrast, the in situ estimate shows regions of subtropical subsidence
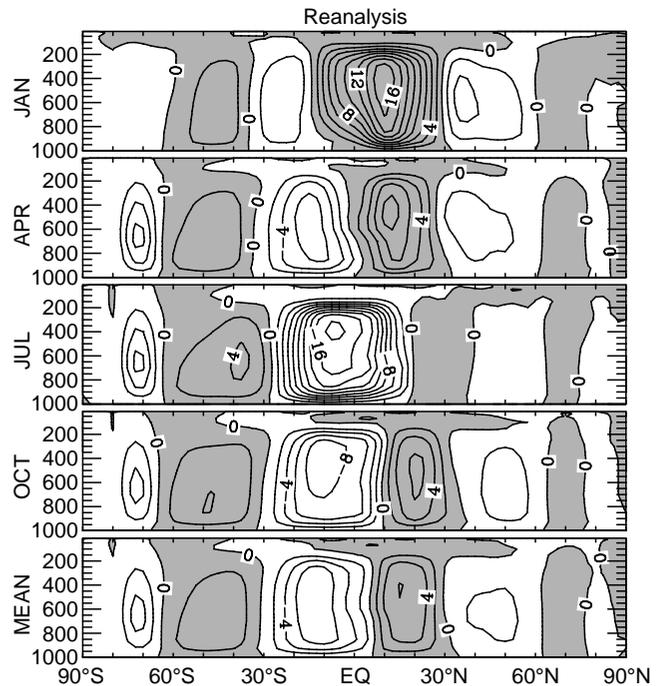

Fig. 3 Same as Fig. 2, except derived from the NCEP/NCAR reanalysis

that are significantly more variable with pressure level, latitude and season.

The Ferrel cells of the reanalysis estimate exhibit considerably less variability in magnitude and latitudinal extent, with the contrast being most striking in the Southern Hemisphere where the in situ estimate shows large annual variability. This greater variability in the in situ estimate might be expected due to seasonal effects projecting onto a fewer number of stations (Fig. 1). This contrast in latitudinal extent and amount of seasonal variability also shows up in the Southern Hemisphere polar cell. The reanalysis shows a narrow polar cell between $65°$–$80°$S throughout the year with a maximum mass flux of between 1.5 and 5.5×10^{10} kg s^{-1}, while the in situ estimate shows a very weak and poorly defined cell. Consistent between these two estimates however is the lack of any appreciable polar cell in the Northern Hemisphere for all seasons. Table 2 presents a measure of correlation between the three different estimates. The values in the second column were determined by calculating the spatial pattern correlations for each month in the annual cycle and then calculating the average of these twelve values. For the reanalysis and in situ estimates, this correlation value is 0.85, indicating that overall these two estimates agree well in the broadest of terms. Spatial maps (latitude by level) of the temporal correlation at each point (not shown) indicate that the poorest temporal correlations are found in the high-latitude Northern Hemisphere and mid- and high-latitude Southern Hemisphere regions.

Figure 4 shows the Hadley circulation climatology derived from the subsampled version of the reanalysis. Comparing this estimate to the previous two shows that many of its features more strongly resemble the in situ estimate. These include: (1) the broader upper tropospheric extent of the northern Hadley cell into the Southern Hemisphere in the January, April and long-term means, (2) the associated limited vertical extent of the southern Hadley cell in these same periods, (3) the greater variability in the latitude of the subsidence regions of the Hadley cells, and (4) the greater annual variability in the southern Ferrel cell. The region of the subsampled estimate that least resembles either of the previous estimates is the polar region of the Southern Hemisphere. Consistent with the reanalysis estimate, the subsampled case shows a relatively stable polar cell. However in contrast to the reanalysis estimate, yet consistent with the in-situ estimate, its latitudinal extent fluctuates considerably. Finally, between $80°$–$90°$S, the subsampled estimate shows a weak but stable clockwise cell with maximum value of about 4×10^{10} kg s^{-1}. The subsampled results in this extreme polar region are based on interpolation from data that are extremely sparse and likely to be significantly biased by the model initialization and physical parametrizations due to the few in situ data sources in the region.
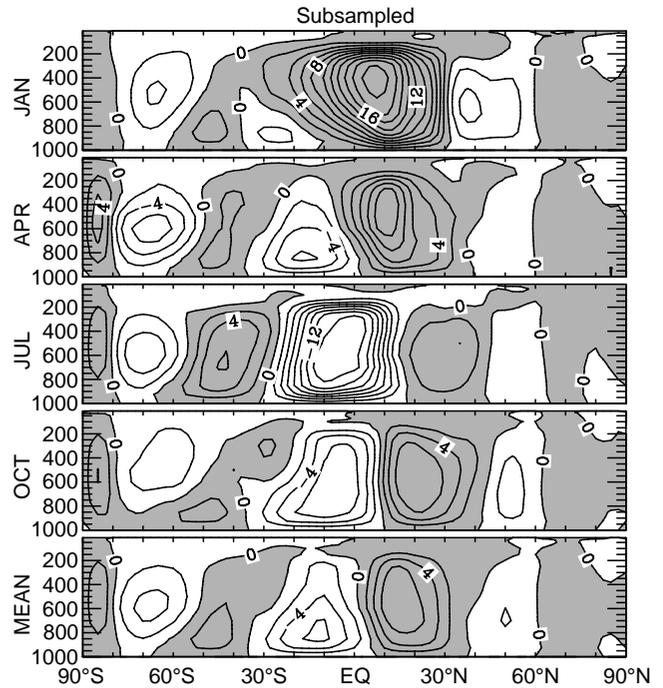

Fig. 4 Same as Fig. 2, except derived from the NCEP/NCAR reanalysis subsampled according to the distribution of data shown in Fig. 1

The differences between the subsampled estimate and the reanalysis estimate indicate the biases that result from computing the Hadley circulation using sparse data. In other words, the similarities between the subsampled and in situ estimates highlighted, which are not shared by the reanalysis estimate, are likely to be artifacts of deriving the Hadley circulation using data from the available set of sparse and irregularly spaced radiosonde stations. Further, the differences between the subsampled and in situ estimates provide some indication of biases introduced by the model or initialization process. Figure 5 shows the differences between the subsampled and reanalysis estimates, and thus provides a measure of the biases introduced by the sparse sampling and associated simplified interpolation scheme. These differences show that the subsampled estimate, relative to the reanalysis estimate, produces a stronger northern Hadley cell, a weaker southern Hadley cell in the upper troposphere, and weaker Ferrel cells in both hemispheres. During some seasons, these differences can produce relative "errors" as large as 100%. Figure 6 shows the differences between the subsampled and the in situ estimates. This figure helps to assess biases in the reanalysis that might result from either the model, the initialization procedure or even ancillary sources of data (e.g., satellite temperature soundings). It shows that the subsampled estimate, relative to the in situ estimate, produces a slightly stronger Hadley circulation, with the relative difference in some seasons as large as 20–30%. Other differences
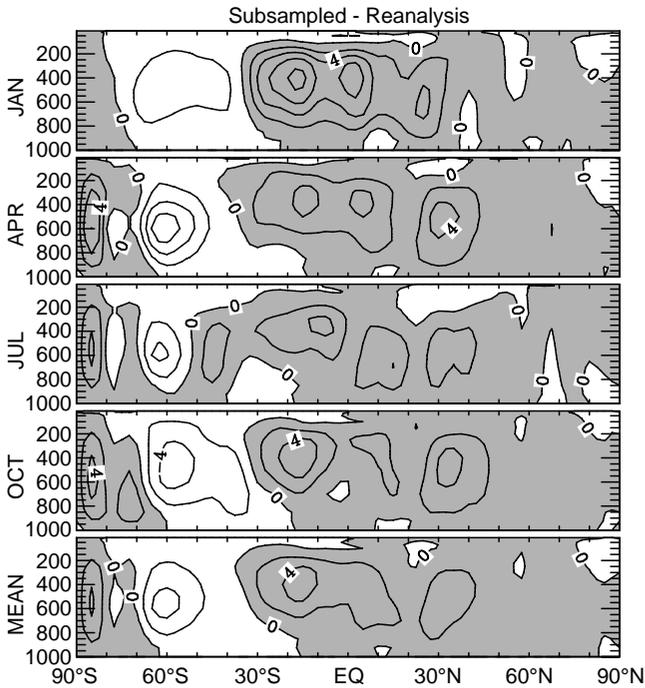
Fig. 5 Difference between the zonal-mean mass stream functions derived from the NCEP/NCAR subsampled reanalysis (i.e., Fig. 4) and the NCEP/NCAR complete reanalysis (i.e., Fig. 3) for mean January, April, July and October conditions as well as the long-term mean for the period 1968–89. Units are in 10^{10} kg s^{-1} and the contour level is 1×10^{10} kg s^{-1}
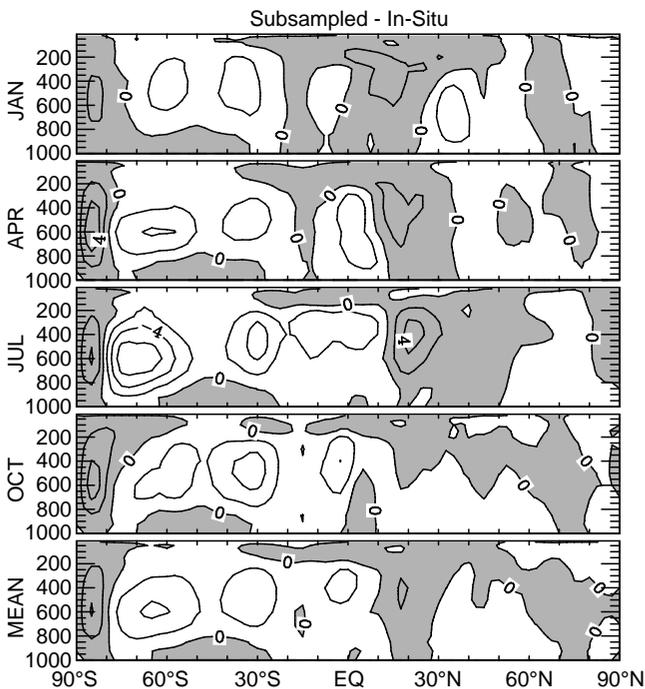
Table 2 Time-averaged spatial-pattern correlations between the in situ, reanalysis and subsampled estimate of the zonal-mean meridional circulation. The values in the second column were determined by calculating the spatial pattern correlations for each month in the annual cycle and then calculating the average of these twelve values. The values in the third column were determined in the same manner, except using the 264 monthly anomaly values. For these calculations, the in situ estimate was interpolated to the same vertical grid used for the reanalysis and subsampled estimates, i.e., 17 levels by 73 latitude points

Estimates	Annual Cycle	Anomalies
Reanalysis and In Situ	0.85	0.16
Reanalysis and Subsampled	0.88	0.26
Subsampled and In-Situ	0.91	0.58

include a weaker southern Ferrel cell and stronger southern polar cell, the magnitudes of which can exceed 100%. However, as mentioned little confidence should be given to all three of the estimates in these regions due to the paucity of data. Examination of the correlations in Table 2 shows that the annual cycle correlation between the reanalysis and subsampled estimates is slightly higher than for the reanalysis and in situ estimates, having a value of 0.88. This slight improvement is due to fact that these two estimates have a common data source (i.e., the reanalysis data). Table 2 also shows that the annual cycle correlation for the in situ and subsampled estimates is 0.91, which is the highest correlation value between the three estimates. This suggests that the sparse sampling, versus reanalysis-induced biases (e.g., model parametrizations, etc.), likely plays a larger role in determining the overall differences between these three Hadley circulation estimates.

4.2 Measures of uncertainty

The results of the comparisons highlight significant differences between the three estimates, some of which are likely attributed to sampling and other differences possibly to the reanalysis procedures and model. To help further assess the influence of the uncertainties introduced by the sampling, we provide some statistical measures of the uncertainty and variability in the meridional circulation estimates. As discussed in Sect.3, the vertically integrated net meridional mass flux (i.e., $\overline{[\bar{v}]}$) is removed at each latitude prior to calculating the mass stream function. Typically, these residuals are small when using monthly data. However, their means and standard deviations can provide some measure of uncertainty for the meridional circulation estimates discussed (Oort and Yienger 1996). Figure 7 shows the means and standard deviations of the residual meridional velocities that were removed from the 264 months of data for each of the three estimates produced. The mean values show that the residuals are indeed
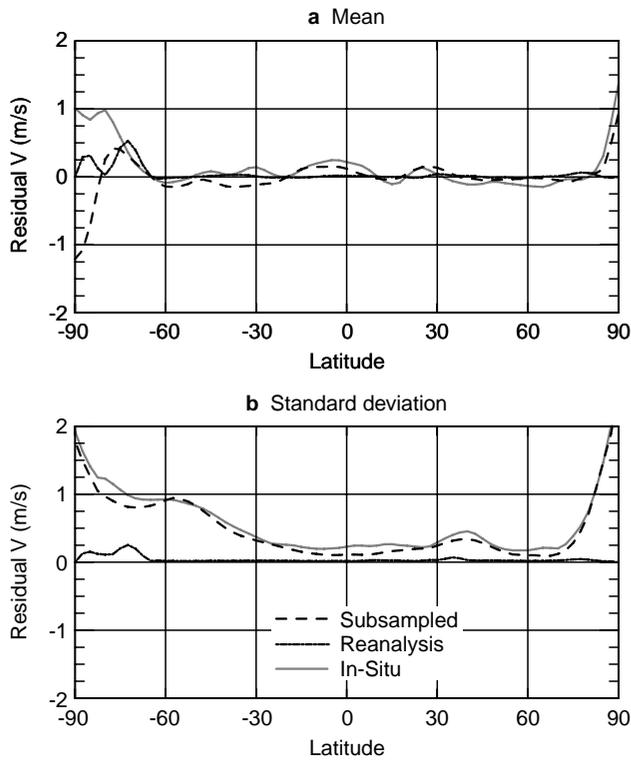

Fig. 6 Same as Fig. 5, except for the difference between the zonal-mean mass stream functions derived from the NCEP/NCAR subsampled reanalysis (i.e., Fig. 4) and the in situ analysis (i.e., Fig. 2)

Fig. 7a,b Means **a** and standard deviations **b** of the residual meridional velocities (i.e., $\overline{[\bar{v}]}$, see Sect. 3) that were removed from the 264 months of data for the in situ (*thick-gray*), reanalysis (*thick black*), and subsampled reanalysis (*dashed*)

Fig. 8 Standard deviations of the anomalies, about the long-term mean annual cycle, of the zonal-mean meridional circulations computed from the in situ (*top*), reanalysis (*middle*) and subsampled (*bottom*) methods. Units are in 10^{10} kg s^{-1} and the contour level is 0.5×10^{10} kg s^{-1}

typically small, on the order of 0.1–0.2 m s^{-1} over the tropical and midlatitude regions. The means for the reanalysis estimate are even smaller, very near 0 m s^{-1}, which is to be expected since all data are used and these data are constrained to conserve the mass of the atmosphere. Near the poles however, the means can be quite large indicating sampling problems in the case of the in situ and subsampled estimate. Note that the mean for Northern Hemisphere reanalysis estimate is near zero which, as just discussed, would be expected, however the mean near the South Pole is quite substantial, near 0.5 m s^{-1}. This is likely due to the fact that many of the lower tropospheric data in this region are based on vertical interpolation from higher altitudes due to the high elevations in the Antarctic.

The standard deviations of the residual meridional velocities suggest similar conclusions regarding regions of uncertainty. The standard deviations for the in situ and subsampled estimates show significant variability in the polar regions, a substantial portion of the Southern Hemisphere (south of about 40 °S), and not surprisingly a small peak in variability in the area of the Northern Hemisphere storm tracks. The standard deviation for the reanalysis is almost zero, except for the far polar region in the Southern Hemisphere and the Northern Hemisphere storm track region. Again, this latter feature is likely related to vertical interpolation to
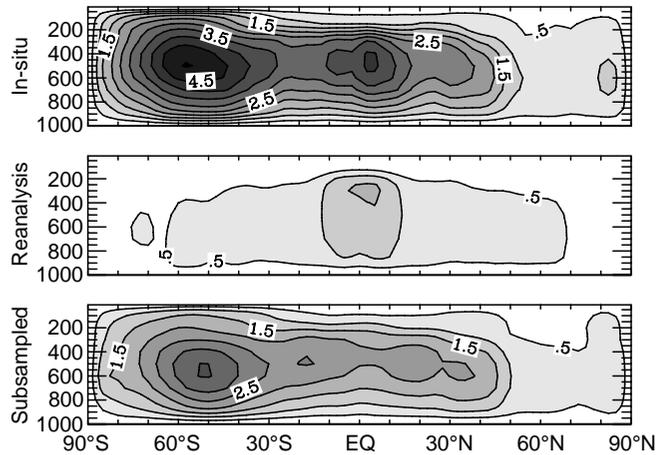
the 1000 hPa level in mountainous regions of the mid-latitudes with the magnitude of the "error" accentuated by midlatitude eddy variability.

An additional measure of uncertainty is illustrated in Fig. 8 which shows the standard deviations of the anomalies (about the annual cycle) of the meridional circulations computed from the in situ, reanalysis and subsampled methods. The variance structures of the in situ and subsampled data are very similar, and both strongly resemble the variance structures presented in Oort and Yienger (1996). Most of the variability is concentrated in the Southern Hemisphere, primarily in the mid-latitudes, with a tongue of high variability extending through the tropics to the Northern Hemisphere subtropics. One minor difference in structure between these two estimates is that the in situ one shows a secondary peak between 10 °S and 15 °N which does not show up in the subsampled estimate. While the spatial structure of these two estimates is similar, the magnitude of the variability in the in situ estimate is about 50% larger than in the subsampled estimate. The reduced variability associated with the subsampled estimate is probably due to: (1) the fact that every monthly average from the subsampled data is based on a full month of "data" whereas the in situ monthly averages can come from as few as 10 observations during the month, and (2) because the data in the subsampled estimate underwent a filtering process via the reanalysis' initialization which would tend to limit the variability.

In contrast to both the in situ and subsampled estimates, the reanalysis estimate shows considerably weaker variability, with a maximum value that is only about 30% (50%) of the maximum value in the subsampled (in situ) estimate. Moreover, the structure is symmetric about the equator with peak values confined

to the deep tropics rather than the southern mid-latitudes. These differences in the variances structure, along with the mean and standard deviations of the residual meridional wind values discussed, indicate the significant changes in variability and in the level of uncertainty introduced into the meridional circulation estimates by the sparse sampling, especially poleward of about 30 °S. While the qualitative aspect of this conclusion is not unexpected, its quantitative consideration leads to very significant differences in perceived interannual variability for the different estimates. In addition, it precludes making rigorous model-data comparisons in this region since the resulting differences are only based on a very small number of stations. More analysis and discussion regarding the changes in variability introduced by subsampling as well as due to model biases will be discussed in the subsection 4.4 in terms of their influence on ENSO-related variability. In the next subsection, analysis is undertaken to ascertain more specific reasons for the differences in the Hadley circulation estimates described in Figs. 2–7.

4.3 Horizontal structure of meridional mass flux

Figure 9 shows the long-term mean meridional mass flux integrated from the 1000 hPa level up to 600 hPa derived from the three meridional wind data sets, i.e. the in situ, reanalysis and subsampled estimates (see Sect. 3). The data are plotted in terms of kg s^{-1} per degree longitude. Thus, summing the data across longitude would result in the 600 hPa mass stream function values shown in Figs. 2–4. These plots provide a means for understanding some of the discrepancies in the derived Hadley circulation estimates shown in Figs. 2–7. A comparison of the large-scale features of these plots shows many similarities. In the southern tropical and subtropical regions, there are northward (i.e., equatorward) flows in the southern Indian Ocean, off the east coast of Australia, and the west coasts of South America and South Africa, and southward (i.e., poleward) flows in the central Pacific, over much of South America and the southwestern subtropical Atlantic. In the northern tropical and subtropical regions, there are southward (i.e., equatorward) flows over northeast Africa, the Arabian Sea, and off the west coasts of North America and northwest Africa, and weak northward (i.e., poleward) flows over southeast Asia, the western Pacific, southern North America and the eastern Atlantic Ocean. In the northern mid- and high latitudes, there are southward flows over northeast Asia and North America, and northward flows over eastern Europe, the northwest Pacific Ocean, and the north Atlantic. In the southern mid- and high latitudes there are southward flows south of Australia and Africa and a region of northward flow over, and to the west, of the Ross Sea. While most of the large-scale features show general agreement there are some notable
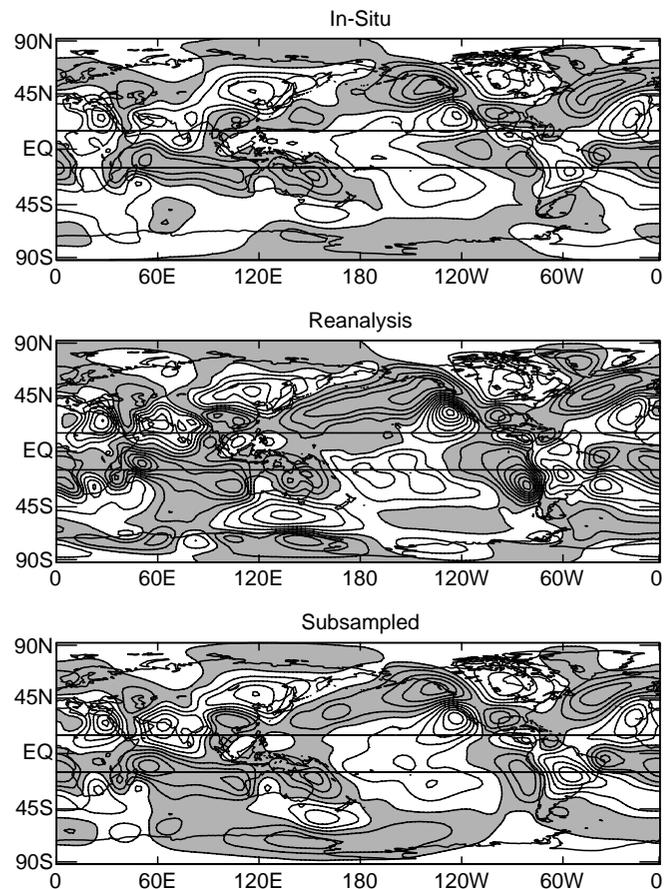

Fig. 9 Long-term mean meridional mass flux integrated from the 1000 hPa level up to 600 hPa from the meridional wind data sets based on the in situ, reanalysis and subsampled analyses (see Sects. 2 and 3). Units are 10^8 kg s^{-1} per degree longitude and the contour level is 2 × 10^8 kg s^{-1}. These units imply that summing the data across longitude would result in the 600 hPa mass stream function values shown in Figs. 2–4. The *two horizontal lines* are at 15 °N and 15 °S

exceptions that end up being responsible for the differences exhibited in the Hadley circulations estimates discussed in Sect. 4.1.

Examining the differences between the subsampled and reanalysis estimates of meridional mass flux (below 600 hPa) highlights the biases introduced into the Hadley circulation computation when using data from sparse, irregularly-spaced locations (e.g., radiosonde network). Overall, the agreement is quite good over most of the Northern Hemisphere owing to the relatively dense network over this hemisphere. In fact, the only region that shows substantial disagreement is a wide area over the Pacific Ocean. Here, the reanalysis shows a tongue of strong northward mass flux extending from Canada to southeast Asia and a region of strong southward mass flux just off the west coast of the United States. In the subsampled estimate both of these features are present with nearly the same spatial structure but with magnitudes that are reduced by about
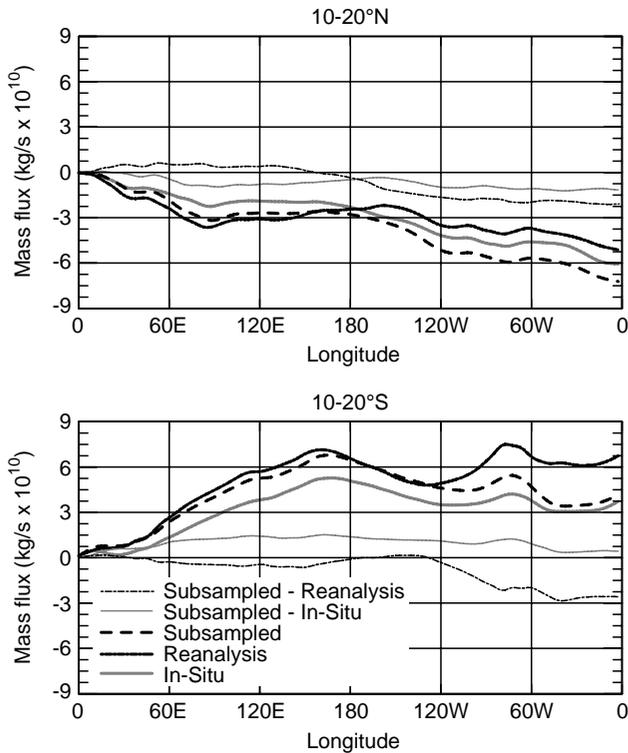
Fig. 10 Running longitudinal-sum of the meridional mass flux (below 600 hPa; i.e., Fig. 9) averaged between 10°–20°N (upper) and 10°–20°S (lower) for the reanalysis (*thick black*), subsampled (*thick dashed*) and in situ (*thick gray*) estimates, along with the differences between the subsampled and reanalysis estimates (*thin dashed*) and the subsampled and in situ estimates (*thin gray*). For reference, see horizontal lines in Fig. 9. The final values of the three running sums (*thick curves*) at 0 °W in each plot are equal to the stream function values at 600 hPa averaged between 10°–20° in Figs. 2, 3 and 4. Non-zero slope values in the differences (*thin curves*) indicate longitudes that contribute to discrepancies in the strength of the Hadley cells shown in Figs. 2–6

30–50%. Just south of these two features, the two mass flux estimates also differ considerably, with the subsampled estimate showing weak southward mass flux over the central tropical Pacific and the reanalysis showing weak northward mass flux. It turns out that this region of disagreement in particular is responsible for the stronger northern Hadley cell in the subsampled estimate compared to the reanalysis estimate.

To illustrate the regions (i.e., longitudes) of discrepancy that contribute to the differences in the three Hadley circulation estimates, Fig. 10 shows the running sums of the meridional mass flux averaged between 10°–20°N (upper) and 10°–20°S (lower) for the reanalysis, subsampled and in situ estimates, along with the differences between the subsampled and reanalysis estimates and the subsampled and in situ estimates. Examination of the mass-flux sums at 10°–20°N for the reanalysis and subsampled estimates, along with their difference, shows that their main area of disagreement occurs between about 150 °E and 150 °W. This is most

easily seen by examining the difference curve and locating longitudes that have the largest non-zero slopes. Due to the wider expanse of southward flux values in the subsampled estimate, the summed mass-flux for the subsampled estimate receives a larger negative contribution in this region. This increase in the low-level southward mass flux ends up being responsible for the stronger northern Hadley cell in the subsampled estimate as compared to the reanalysis estimate (Figs. 3–5). While this result is certainly dependent on the type of interpolation performed on the sparse in situ data, it provides an example of what the sign and magnitude of a typical error might be in an in situ derived calculation of the Hadley circulation. It is worth noting that the regions of largest discrepancy between reanalysis and sub-sampled in the tropics, namely the central North Pacific, the central and eastern South Pacific, and the southern Indian Ocean correspond well to the areas of largest discrepancies found by Soden and Lanzante (1996). The latter authors examined the effects of the sparse radiosonde network on upper tropospheric humidity through the use of subsampling and spatial analysis of satellite data using techniques very similar to those used herein. The pattern of discrepancy shown in their Fig. 12c highlights these problem areas.

As might be expected, comparing the meridional mass-flux values between the reanalysis and subsampled estimates in the Southern Hemisphere of Fig. 9 shows even more discrepancy, with only the grossest of features being similar. Most notable in the tropics, is the slightly weaker northward flow over the southern Indian Ocean and the significantly weaker northward flow over the southeastern Pacific Ocean in the subsampled estimate. The lower plot in Fig. 10 shows that the latter discrepancy ends up being the main contributor to the weaker southern Hadley cell in the subsampled estimate (Figs. 3–5). Given the lack of data in the mid- and high-latitude regions of the Southern Hemisphere (Fig. 1), it is not surprising that the two show significant disagreement in this region. For example, the region to the south and southeast of Australia shows very poor agreement. This pronounced disagreement in the meridional mass flux is consistent with the very different meridional circulation patterns in the southern polar region of Figs. 3 and 4.

Examining the differences between the subsampled and in situ estimates of meridional mass flux below 600 hPa highlights the biases introduced into the Hadley circulation computation by the reanalysis (i.e., from the model, initialization procedures and in-direct data sources). Overall, the agreement in the spatial structure is quite good, even in much of the Southern Hemisphere. The principle difference is that, in many areas, the mass flux values from the subsampled analysis are stronger than those in the in situ analysis. For example, the southward flows over the Arabian Sea, eastern North Pacific, northern North America, central

South America, and south of Australia are all about 20–40% larger in the subsampled estimate. Likewise for the northward flows over the western and central North Pacific, north Atlantic, subtropical Indian Ocean and southeastern Pacific. These enhanced lower tropospheric flows are responsible for the larger Hadley circulation in the subsampled estimate as compared to the in situ estimate (Figs. 2, 4, and 6).

Comparing the in situ and subsampled estimates in Fig. 10 for the region between $10°$–$20°$N shows that as we proceed from east to west, the differences in southward flow over the Arabian Sea and northward flow over the western Pacific almost cancel, leaving the total southward mass flux about the same upon reaching the dateline. However, the magnitude of the difference occurring in the eastern Pacific ends up accounting for the larger total southward mass flux, and thus the stronger northern Hadley cell, in the subsampled versus in situ analyses (Figs. 2, 4, and 6). For the region between $10°$–$20°$N, the slightly stronger northward mass flux in the subsampled estimate compared to the in situ estimate results from the enhanced northward flows over the subtropical Indian Ocean and southeastern Pacific Ocean, with the enhanced southward flows over the central tropical Pacific and South America not quite being able to compensate.

This comparison between the subsampled and in situ estimates shows that the lower tropospheric flows tend to be enhanced in the subsampled analysis relative to the in situ estimates by about 20–40%. As shown earlier, this results in about a 10–20% enhancement in the subsampled Hadley circulation. It is of interest to know if this mass-flux bias in the lower troposphere occurs in some systematic manner. For example, is it primarily due to a difference in the COADS ship and 10 m reanalysis winds, each used to represent near-surface ocean winds, or is it due to a difference in the meridional winds at higher levels? Based on a detailed examination of the locations with in situ data, that are near areas of large disagreement (highlighted earlier), it was found that the meridional wind biases have very little overall systematic structure with height. For example, the larger northward mass flux in the north Atlantic results from slightly enhanced surface winds ($\sim 0.3 \, \text{m s}^{-1}$), with the difference growing with height above the surface, being about $1 \, \text{m s}^{-1}$ near $600 \, \text{hPa}$. In contrast, the enhanced northward mass flux in the north Pacific results from a meridional wind difference of about $1 \, \text{m s}^{-1}$ at the surface that diminishes with height.

The enhanced northward flow in the southeast subtropical Indian Ocean and the enhanced southward flow in the eastern north Pacific come about primarily from meridional wind biases occurring above $900 \, \text{hPa}$ with the surface winds showing good agreement in the mean. Over the southeastern Pacific Ocean and the Arabian Sea, the meridional wind changes sign between the surface and $600 \, \text{hPa}$. In both cases, both the surface

wind and lower tropospheric winds contribute to the differences. In the southeastern Pacific Ocean, the northward surface wind in the subsampled analysis (which determines the sign of the mass flux) is biased high by about $0.5 \, \text{m s}^{-1}$, while the southward winds at all higher levels (up to $600 \, \text{hPa}$) are also too weak by about the same amount. Over the Arabian Sea, the southward lower tropospheric wind in the subsampled analysis (which determines the sign of the mass flux) is biased high by about $1 \, \text{m s}^{-1}$, while the northward surface winds are smaller by about $0.5 \, \text{m s}^{-1}$. While these comparisons are not detailed enough to suggest the physical (or algorithmic) reasons behind the biases in the subsampled reanalysis relative to the in situ data, they do suggest that overall the strength of the circulation in the lower atmosphere is enhanced in the reanalysis winds relative to the in situ observations, at least in places where input data to the analysis is available.

4.4 Interannual variability

In the study by Oort and Yienger (1996), the influence of ENSO in the Hadley circulation was examined by computing the anomalous Hadley circulation averaged over the five warmest El Nino events minus the same quantity averaged over the five coldest La Nina events. Their calculation was based on the period 1964–89 and a time series of eastern Pacific large-scale SST anomalies. Their results showed a $3 \times 10^{10} \, \text{kg s}^{-1}$ intensification of the northern Hadley cell, and a $4 \times 10^{10} \, \text{kg s}^{-1}$ intensification of the southern Hadley cell for warm versus cold conditions. Studies by Trenberth (1997) and Sun and Trenberth (1998) indicate that associated with El Nino are significant increases in atmospheric meridional heat transport. This enhanced heat transport could be attributed to a stronger meridional circulation and/or the stronger equator-to-pole temperature gradient present during El Nino. The result by Oort and Yienger (1996) suggests that the former plays at least some role. In fact, their result suggests about a 25–75% increase in the strength of the meridional circulation when considering the magnitude of their ENSO enhancement to the Hadley circulation in conjunction with its climatological variation (i.e., Fig. 2). However, the results in the previous section concerning biases in the Hadley circulation climatology induced by the use of sparse sampling raise a question regarding their influence on the assessment of ENSO-related Hadley circulation variability.

Figure 11 shows a normalized index of SST variability from the eastern tropical Pacific. This time series represents a surrogate measure of ENSO variability. Figure 12 shows the difference in the anomalous zonal-mean meridional circulation between El Nino and La Nina periods, where El Nino (La Nina) periods are defined as the months when the normalized SST
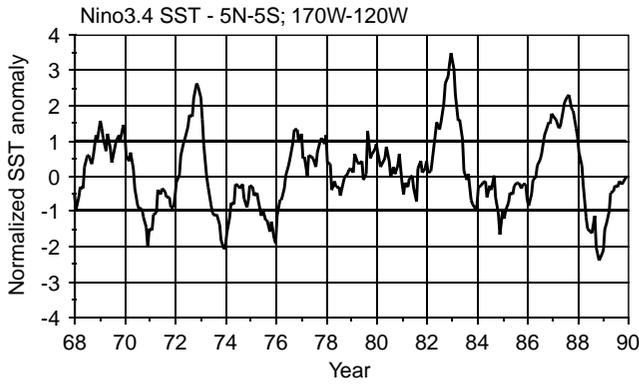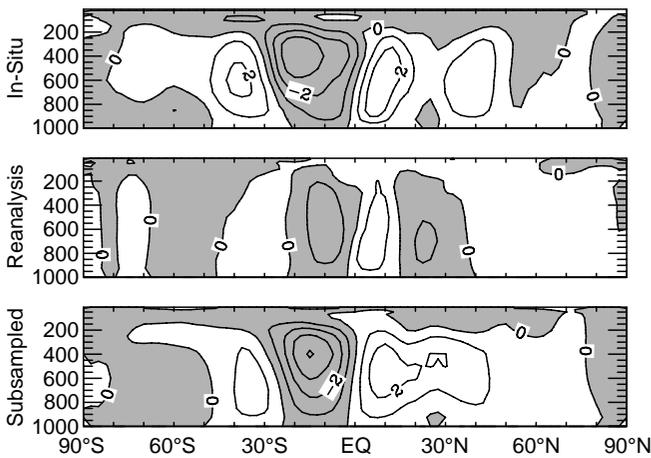
Fig. 11 Sea surface temperature anomaly averaged over the eastern tropical Pacific "Nino 3.4" region (5 °N–5 °S, 170 °W–120°W). The data have been normalized using the standard deviation of the time series between 1950 and 1997 (= 0.87 °C)

Fig. 12 Difference in the anomalous zonal-mean meridional circulation between El Nino and La Nina periods. El Nino (La Nina) periods are defined as the months when the normalized "Nino 3.4" sea surface temperature was greater (less) than 1.0; see Fig. 11

from the in situ estimate that suggests that the discrepancy between the in situ and reanalysis estimates is strongly associated with the reliance on sparsely sampled data. This conclusion is also reflected in the time-averaged, spatial-pattern correlations of the interannual anomalies shown in the third column of Table 2. These values were calculated by determining the spatial pattern correlations of the anomalies for each month and then averaging these 264 values together. Note that the correlation is relatively low between the reanalysis and in situ estimate (0.16), it increases slightly for the reanalysis and subsampled estimates (0.26) due to the fact these two estimates share the same data source, and then it increases significantly for the subsampled and in situ estimates (0.58), indicating the large influence associated with the sparse sampling.

Figure 13 shows the in situ, reanalysis and subsampled derived differences in meridional mass flux integrated from 1000 hPa up to 600 hPa between anomalies averaged during the El Nino periods and those averaged during the La Nina periods. The data are plotted in terms of kg s^{-1} per degree longitude. Thus, summing the data across longitude would result in the 600 hPa mass streamfunction anomalies shown in Fig. 12. The most obvious influence of ENSO in the in situ map is the area of strong equatorial mass convergence extending from about 140 °E to about 140 °W. The next largest perturbation in mass-flux is a region of northward flow located in the northeast Pacific Ocean. This region of northward intensification, along with the region of southward intensification to the southwest, result from the amplification of the Aleutian Low that is typically associated with El Nino.

While the subsampled El Nino minus La Nina mass flux map in Fig. 13 shows a high degree of similarity to the in situ map, the map based on the reanalysis data show several areas of significant discrepancy. The most prominent are the equatorial areas that exhibit strong mass divergence to the west and east of the large-scale area of mass convergence described. These divergent areas are located over the Indian Ocean in one case and extend from the eastern Pacific Ocean across to the Atlantic Ocean in the other. In the case of the divergent area over the Indian Ocean, the structure and intensity of the northward flow north of the equator in the in situ and subsampled estimates are fairly similar to the reanalysis estimate due to the relatively high number of observations available in this region (Fig. 1). However, the structure and intensity of the region of southward flow south of the equator is poorly represented in the in situ and subsampled estimates presumably due to the paucity of data in southern Indian Ocean. Similar discrepancies hold for the divergent area in the western hemisphere, with the region of southward (northward) mass flow over the southeastern Pacific (northern tropical Atlantic) having a magnitude significantly (moderately) less in the in situ and subsampled estimates compared to the reanalysis estimate.
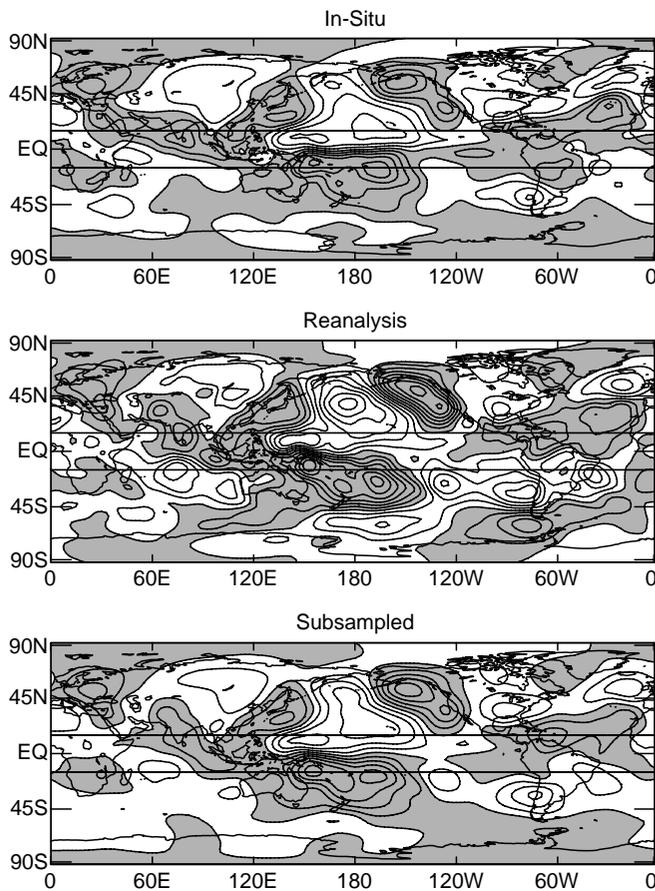
index in Fig. 11 is greater (less) than 1.0. The difference plot for the in situ estimate shows a Hadley intensification of about 2×10^{10} kg s^{-1} and 3×10^{10} kg s^{-1} for the northern and summer Hadley cells, respectively. The structures and relative magnitudes of the intensification is very similar to Oort and Yienger's result. The magnitude is slightly weaker due to the fact that they examined summer and winter seasons separately. This resulted in about a 10° northward shift in the position of their intensified northern-summer Hadley cells relative to their result for northern winter; averaging their two seasonal values would produce a result very similar to that shown in Fig. 12. The difference plot for the reanalysis estimate shows a Hadley intensification of only about 1×10^{10} kg s^{-1} for each hemisphere, a reduction of about 50% and 70% for the Northern and Southern Hemispheres, respectively. The difference plot for the subsampled result strongly resembles that

Fig. 13 Same as Fig. 9, except for the differences between anomalies averaged during El Nino and La Nina conditions. El Nino (La Nina) periods are defined as the months when the normalized "Nino 3.4" sea surface temperature was greater (less) than 1.0; see Fig. 11
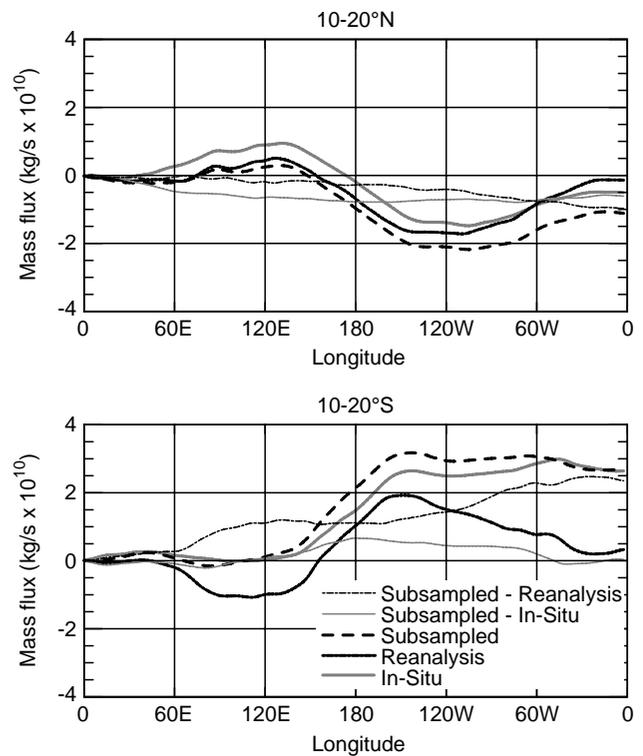

Fig. 14 Same as Fig. 10, except applied to Fig. 13, i.e. the differences between anomalies averaged during El Nino and La Nina conditions. El Nino (La Nina) periods are defined as the months when the normalized "Nino 3.4" sea surface temperature was greater (less) than 1.0; see Fig. 11

The influence of these differences on the implied changes to the Hadley circulation are demonstrated in Fig. 14 which is similar to Fig. 10 except applied to the El Nino minus La Nina meridional mass flux maps shown in Fig. 13. Comparing the running sums of mass flux at $10°–20°N$ shows that the main difference between the subsampled and reanalysis estimates largely results from the weaker contribution in the subsampled estimated of northward flow over the Atlantic region. This results in a stronger interannual change in the northern Hadley cell mass flux implied for the subsampled case as compared to the reanalysis case (in this latitude range about 1×10^{10} kg s^{-1} as compared to 2×10^{10} kg s^{-1}). Comparing the running sums for the in situ and reanalysis estimates shows this weaker northward contribution in the Atlantic also occurs in the in-situ case but is offset by a stronger northward contribution coming from the region around the Arabian Sea. In the case of the running sums at $10°–20°S$, the reanalysis curve shows an area of strong southward mass flux around $120°E$, a very strong area of northward mass flux around $180°$, and then an area of southward flow centered around $90°W$.

Combined, the regions of northward and southward mass flux nearly cancel leaving very little net effect on the strength of the southern Hadley cell. On the other hand, the weaker southward flows in the in situ and subsampled estimates over the Indian and eastern Pacific Oceans prevents this cancellation leaving a very large net effect on the strength of the southern Hadley cell.

A comparison of the subsampled and in situ estimates in Fig. 13 highlights aspects related to the biases in the reanalysis product. Similar to the comparison in the previous section of the long-term mean meridional mass flux, the subsampled El Nino minus La Nina meridional mass flux shows a slightly enhanced lower tropospheric circulation relative to the in situ estimate. The region of southward flow north of the equator and the region of northward flow south of the equator are each about 20% larger in the subsampled estimate. A similar size increase occurs for many of the other regions of relatively high meridional mass fluxes. Thus, in addition to the enhancement in the long-term mean meridional mass flux values (Sect. 4.3), the interannual variations in the meridional circulation appear to be enhanced as well. Together these results suggest that the meridional circulation in the tropics, and in some cases in the mid-latitudes as well, is stronger in the

reanalysis as compared to in situ data, at least in places where in-situ data are available.

5 Summary and conclusions

The objective of this study was to compare estimates of the zonal-mean meridional circulation produced from a long-record reanalysis product to that produced directly from in situ observations using traditional techniques. It is understood that both of these estimates suffer from their own biases and uncertainties. Thus, part of the challenge of this study was to try and construct a framework for producing a worthwhile comparison from which useful and meaningful inferences could be drawn. Our approach was to produce a third estimate by subsampling the reanalysis data set at the locations where observed data exists (Fig. 1; compare witt Oort 1983), and then estimate the circulation from this subset of data in the same way the in situ estimate is produced (i.e., with some form of objective analysis). This subsampled estimate suffers from both the sparse data limitation as well as the biases associated with the reanalysis (e.g., from model parametrizations, initialization procedures, and indirect sources of data such as satellite retrievals). By comparing the subsampled and reanalysis estimates, inferences could be drawn regarding the biases in the conventional in situ estimates due to sparseness of the data sources (i.e., radiosonde network). By comparing the subsampled and in situ estimates, inferences could be drawn regarding the biases in the reanalysis estimates. Understandably, within this framework, these latter inferences could only be associated with locations where actual in situ observations exist, and thus it is likely that they would underestimate, or possibly not altogether apply, to regions void of in situ data. Implicit within this objective and associated analysis, is an underlying goal of trying to narrow the gap between truth and previous estimates of the zonal-mean meridional circulation.

The in situ estimate was constructed from monthly radiosonde and COADS surface ship observations of meridional wind for the period from 1968 to 1989. The reanalysis and subsampled estimates were constructed from monthly NCEP/NCAR reanalysis data from the same period. While the climatologies from the three estimates (Figs. 2–4) all showed the expected large-scale features, the detailed aspects of their representations, including the strengths of the circulations, differed significantly. For example, the principle qualitative differences between the in situ and reanalysis estimates include: (1) the southern Hadley cells in the reanalysis consistently extend up to 200 hPa, whereas the bulk of the circulation for the in situ estimate tends to be confined to the lower half of the troposphere allowing the northern cell to extend further into the Southern Hemisphere at upper levels, (2) the reanalysis exhibits more well-defined and consistent poleward limits of the Hadley cells, with the main regions of subsidence almost always occurring at 30 °N and 30 °S, (3) the Ferrel cells and southern polar cell in the reanalysis estimate exhibit considerably less variability in magnitude and latitudinal extent, and (4) the reanalysis exhibits a narrow polar cell between 65°–80 °S throughout the year while the in situ estimate exhibits a very weak and poorly defined cell. Comparing the subsampled estimate to the in situ and reanalysis estimates shows that many of its features more strongly resemble the in situ estimate. Specifically, the qualitative differences described between the in situ and reanalysis estimate are not as evident when comparing the in situ and subsampled estimates. This indicates that these qualitative differences are, to a large degree, associated with the sparse sampling and simplified interpolation schemes associated with the in situ and subsampled estimates.

Quantitative comparison shows that the subsampled estimate, relative to the reanalysis estimate, produces a stronger northern Hadley cell ($\sim 20\%$), a weaker southern Hadley cell (mainly in the upper troposphere; ~ 20–60%), and weaker Ferrel cells in both hemispheres (Figs. 3–5). Long-term mean maps of meridional mass flux below 600 hPa were examined to understand the reason for these differences (Figs. 9 and 10). It was found that the stronger northern Hadley cell in the subsampled estimate primarily stems from the poor sampling of the central and western subtropical North Pacific. This poor sampling is responsible for producing a weakened northward flow in this region, leading to an overall enhancement in the equatorward mass flux (i.e., northern Hadley cell) in the subsampled estimate relative to the reanalysis. The weaker southern Hadley cell in the subsampled estimate relative to the reanalysis estimate primarily stems from the poor sampling in the southeast Pacific, and to a lesser extent the southern subtropical Indian Ocean. Both these regions make significant contributions to the low-level northward mass flux in the southern Hadley cell, and their weakened representation in the subsampled, and presumably the in situ, estimate produce weakened southern Hadley cells. The radiosonde sparseness in these regions was similarly found by Soden and Lanzante (1996) to be areas of maximal bias in monitoring upper tropospheric humidity. Likewise, the weaker Ferrel cells in the subsampled estimate relative to the reanalysis estimate also results from poorly resolved regions of significant low-level poleward flow over the oceans (e.g., north Pacific and central south Pacific and Atlantic).

Comparisons between the subsampled and in situ estimates suggest that the subsampled estimate produces a slightly stronger Hadley circulation in both hemispheres, with the relative difference in some seasons as large as 20–30% (Figs. 2, 4 and 6). This

enhanced overall Hadley circulation is associated with an overall enhancement in the strength of the circulation, indicated here by a strengthening of the meridional mass flux below 600 hPa (Figs. 9 and 10). Since the data for each of these estimates comes from generally the same locations, this enhancement in the circulation is likely attributable to biases in the reanalysis. However, in this study, the analysis of these biases is limited to areas where in situ data exist and therefore little can be inferred regarding the biases in regions void of in situ data, although it is likely they would have the same sign and have a similar or greater magnitude. The possibility exists that part of the differences between the in situ and subsampled analyses are due to biases in the in situ data that do not impact the reanalysis due to the use of additional data sources. However, it is expected that such biases would still represent a smaller fraction of error than the reanalysis procedure itself (i.e., model dependencies), particularly for the case of wind measurements.

Additional analysis was undertaken to try and ascertain if the biases in the low-level flow between the in situ and subsampled analyses showed a systematic behavior with height (e.g., always associated with near-surface flow). However, no such systematic behavior could be identified other than the general suggestion that the strength of the low-level flow in the reanalysis, in regions with in situ data, is more energetic than that suggested by the monthly in situ observations. By considering these conclusions regarding sparse sampling and model biases, it might be reasonable to assume that the true Hadley circulation has a spatial structure highly similar to the reanalysis estimate provided here but with an overall strength that is a bit weaker.

ENSO-related changes to the Hadley circulation in the three estimates were also performed. Specifically, composite El Nino minus La Nina anomalies of the zonal-mean meridional circulation were computed and compared (Figs. 11 and 12). The difference plot for the in situ estimate shows a Hadley intensification of about 2×10^{10} kg s^{-1} and 3×10^{10} kg s^{-1} for the northern and summer Hadley cells, respectively (similar to Oort and Yienger 1996). However, the difference plot for the reanalysis estimate indicates a Hadley intensification of only about 1×10^{10} kg s^{-1} for each hemisphere, a reduction of about 50% and 70% for the Northern and Southern Hemispheres, respectively. Interestingly, the difference plot for the subsampled result strongly resembles, in structure and magnitude, that from the in situ estimate which suggests that the discrepancy between the in situ and reanalysis estimates is strongly associated with the reliance on sparsely sampled data. Examination of the El Nino minus La Nina anomalous values of meridional mass flux below 600 hPa (Figs. 13 and 14) shows that all three estimates capture the large-scale region of low-level equatorial convergence near the dateline. However, the in situ and subsampled

estimates fail to effectively reproduce the large-scale areas of equatorial mass divergence to the west and east this convergence area. These low-level divergent areas are located over the Indian Ocean in one case and extend from the eastern Pacific Ocean across to the Atlantic Ocean in the other. In the reanalysis, the poleward mass fluxes associated with these divergent areas nearly cancel the equatorward flow in the central Pacific. However, due to the weakened representation of the low-level poleward flows in the subsampled and in situ analyses, this cancellation is not as complete, leaving a fairly substantial net ENSO effect on the derived Hadley circulation.

In addition to ENSO-related interannual variability, total month-to-month interannual variability was also computed for the three estimates in terms of their standard deviations about the annual cycle (Fig. 8). The variance structure of the in situ and subsampled meridional circulations show a high degree of spatial similarity, although the magnitude of the in-situ estimate is about 50% larger than in the subsampled estimate. Most of the variability is concentrated in the Southern Hemisphere, primarily in the mid-latitudes, with a tongue of high variability (2–4×10^{10} kg s^{-1}) extending through the tropics to the Northern Hemisphere subtropics. In contrast to both the in situ and subsampled estimates, the reanalysis estimate shows considerably weaker variability, with a maximum value that is only about 30% (50%) of the maximum value in the subsampled (in situ) estimate. Moreover, the structure is symmetric about the equator with peak values confined in the deep tropics rather than the southern mid-latitudes. While some aspects of these differences might be expected due to the sparse in situ sampling, their quantitative consideration leads to very significant differences in perceived interannual variability for the different estimates. Finally, these differences in the structure and magnitude of the variances, along with additional measures of uncertainty discussed in Sect. 4.2 (Fig. 7), indicate considerable differences in the level of uncertainty introduced into the meridional circulation estimates by the sparse sampling, especially poleward of about 30 °S. This greater level of uncertainty in the in situ and subsampled estimates warrants some caution regarding the inferences made between these two estimates and what they imply for biases associated with the reanalysis. Thus, the conclusions regarding the reanalysis biases have to be considered in light of other reanalysis validation efforts.

providing useful comments on the earlier versions of this work, as well as thank Gabriel Lau for his support and encouragement with this study. This study's analysis greatly benefited from the use of the TeraScan software analysis system, a product of SeaSpace Corporation, San Diego, CA.

References

Buchan A (1889) Report on atmospheric circulation. Report on the scientific results of the exploring voyage of the HMS Challenger, 1873–76. Physics and Chemistry, vol 2. HM Stationery Office (25)

Elliot WP, Gaffen DJ (1991) On the utility of radiosonde humidity archives for climate studies. Bull Am Meteorol Soc 72:1507–1520

Emanuel KA (1995) On thermally direct circulations in moist atmospheres. J Atmos Sci 52:1529–34

Gaffen DJ (1994) Temporal inhomogeneities in radiosonde temperature records. J Geophys Res 99:3667–3676

Hack JJ, Shubert WH, Stevens DE, Kuo HC (1989) Response of the Hadley circulation to convective forcing in the ITCZ. J Atmos Sci 46:2957–2973

Hadley G (1735) Concerning the cause of the general trade-winds. Philos Trans 29:58–62

Held IM, Hou AY (1980) Nonlinear axially symmetric circulations in a nearly inviscid atmosphere. J Atmos Sci 37:515–533

Hou AY, Lindzen RS (1992) The influence of concentrated heating on the Hadley circulation J Atmos Sci 49:1233–1241

Kalnay E, Kanamitsu M, Kistler R, Collins W, Deaven D, Gandin L, Iredell M, Saha S, White G, Woollen J, Zhu Y, Chelliah M, Ebisuzaki W, Higgins W, Janowiak J, Mo K, Ropelewski C, Wang J, Leetmaa A, Reynolds R, Jenne R, Joseph D (1996) NCEP/NCAR 40-year reanalysis project. Bull Am Meteorol Soc 77:437–471

Lindzen RS, Hou AY (1988) Hadley circulations for zonally averaged heating centered off the equator. J Atmos Sci 45:2416–2427

Lorenz EN (1967) The nature and theory of the general circulation in the atmosphere. WMO Publ 218

Maury MF (1855) The physical geography of the sea. New York, Harper, 287 pp (63)

Newell RE, Kidson JW, Vincent DG, Boer GJ (1972) The general circulation of the tropical atmosphere, vol 1, 2. The MIT Press

Oort AH (1978) Adequacy of the rawinsonde network for global circulation studies tested through numerical model output. Mon Weather rev 106:174–195

Oort AH (1983) Global atmospheric circulation statistics, 1958–1973. NOAA Prof. Pap 4. US Government Printing Office, Washington, D.C., 180 pp

Oort AH, Rasmusson EM (1970) On the annual variation of the monthly mean meridional circulation. Mon Weather Rev 98:423–442

Oort AH, Yienger JJ (1996) Observed interannual variability in the Hadley circulation and its connection to ENSO. J Clim 9:2751–2767

Parker DE, Cox DI (1995) Towards a consistent global climatological rawindsonde data-base. Int J Clim 15:473–496

Schneider EK (1977) Axially symmetric steady-state for instability and climate studies. Part II. Nonlinear calculations. J Atmos Sci 34:280–296

Schneider EK (1987) A simplified model of the modified Hadley circulation. J Atmos Sci 44:3311–3328

Schneider EK, Lindzen RS (1977) Axially symmetric steady-state for instability and climate studies. Part I. Linearized calculations. J Atmos Sci 34:263–279

Schubert SD, Pfaendtner J, Rood R (1993) An assimilated data set for Earth science application. Bull Am Meteorol Soc 74:2331–2342

Schwartz BE, Doswell CA (1991) North American rawinsonde observations: problems, concerns and a call to action. Bull Am Meteorol Soc 72:1885–1896

Soden BJ, Lanzante JR (1996) An assessment of satellite and radiosonde climatologies of upper-tropospheric water vapor. J Clim 9:1235–1250

Sun DZ, Trenberth KE (1998) Coordinated heat removal from the tropical Pacific during the 1986–87 El Nino. Geophys Res Let 25:2659–2662

Trenberth KE (1991) Climate diagnostics from global analysis: conservation of mass in ECMWF analyses J Clim 4:707–722

Trenberth KE (1997) The heat budget of the atmosphere and ocean. First Int Conf on Reanalyses, Silver Spring, MD 27–31 October, 1997

Trenberth KE, Olson JG (1989) Temperature trends at the South Pole and McMurdo Sound, J Clim 2:1172–1182

Trenberth KE, Solomon A (1994) The global heat balance: heat transports in the atmosphere and ocean. Clim Dyn 10:107–134

van den Dool HM, Saha S, Schemm J, Huang J (1997) A temporal interpolation method to obtain hourly atmospheric surface pressure tides in reanalysis 1979–1995: J Geophys Res 102:22013–22024

Woodruff SD, Slutz RJ, Jenne RL, Steurer PM (1987) A comprehensive ocean-atmosphere data set. Bull Am Meteorol Soc 68:1239–1250